Journal of Power Sources 205 (2012) 467–473

Contents lists available at SciVerse ScienceDirect

Journal of Power Sources

journal homepage: www.elsevier.com/locate/jpowsour

Short communication

The effect of metal silicide formation on silicon nanowire-based lithium-ion battery anode capacity

Jeong-Hyun Cho*, Xianglong Li, S. Tom Picraux**

The Center for Integrated Nanotechnologies, Los Alamos National Laboratory, Los Alamos, NM 87545, USA

ARTICLE INFO

Article history:
Received 31 October 2011
Received in revised form
23 December 2011
Accepted 1 January 2012
Available online 9 January 2012

Keywords:
Anode
Chemical vapor deposition
Lithium-ion battery
Metal silicide
Silicon nanowire

ABSTRACT

There is great interest in one-dimensional (1D) nanostructures that allow lateral relaxation and can be used to reduce pulverization of a silicon-based anode material. However, the growth of high density arrays of silicon nanowires (SiNWs) on metal current collectors using a chemical vapor deposition (CVD) processing is challenging due to competing metal silicide formation during the Si nanowire growth process. An issue with the metal silicide formation is that Si is consumed and this reduces the overall specific capacity as well as the rate capability of a silicon nanowire-based anode material. Here, we demonstrate high density, electrically contacted Si nanowire growth on stainless steel substrates (metal current collectors) with minimal unwanted substrate-silicide formation for high Li ion battery performance. These high-purity silicon nanowire-based anodes show average high specific capacities of 3670 mA h g^{-1} at 0.2 C and 3448 mA h g^{-1} at 0.5 C over 40 cycles. Moreover, the high-purity silicon nanowires are demonstrated to reach extremely high capacities at high cycle rates (1912 mA h g^{-1} and 997 mA h g^{-1} at 10 C and 20 C, respectively).

1. Introduction

A miniature rechargeable battery with maximized energy and power density is in high demand for portable electronic systems and electric vehicles. Among the many different kinds of rechargeable batteries, lithium-ion batteries are widely used in consumer electronics because of their relatively high energy and power density, lack of memory effects, and low self-discharge. However, the energy density is not high enough for long-term operations on a single charge. Further, the pace at which the energy capacity of batteries is improving is not fast enough to mitigate the energy consumption of new electronic systems. The anode electrode of a commercial lithium-ion battery is made of graphite and the theoretical capacity is 372 mA h g^{-1} [1]. The energy capacity of the anode can be increased up to an order of magnitude by using Si (4200 mA h g^{-1}) [2]; however, the mechanical stress due to the huge volume increase of 300% upon lithiation quickly degrades the electrode and leads to partial loss of electrical contact between the anode material (Si) and current collector [3]. As a result, these effects lead to capacity fade during cycling (poor cycling performance). Recently, there is great interest in one-dimensional (1D) nanostructures that allow lateral relaxation and can be used to reduce pulverization of a silicon-based anode material [4–7].

Silicon nanowires (SiNWs) grown with a chemical vapor deposition (CVD) synthesis process directly onto metal current collectors have shown particular promise for improved electrical connection between an anode material (each SiNW) and the metallic current collector while providing for high capacity [4–6]. However, it is challenging to grow 100 weight percent (wt%) of SiNWs directly on metal substrates (metal current collectors) due to wetting of the catalyst which limits NW nucleation and to competing unwanted substrate-silicon reactions forming metal silicides. An issue with the metal silicide formation is that Si is consumed and this reduces the overall specific capacity as well as the rate capability of a silicon nanowire-based anode material. Minimization of metal silicide formation during Si nanostructure synthesis and the resulting effect on electrochemical performance is a fundamental problem which must be solved in implementing high performance silicon and/or silicon composite anodes. However, previously reported work has not examined the consequences of such silicon–electrode interactions. In the present study, we observe a significant effect of metal silicide formation between the silicon NWs and metal electrode on the electrochemical performance of silicon nanowire based Li ion half-cells. We demonstrated a route to minimize silicide formation and show how this leads to enhancement in the rate capability of silicon nanowires as well as increased specific capacity when

* Corresponding author. Tel.: +1 505 665 4240; fax: +1 1 505 665 9030.
** Corresponding author.
E-mail addresses: jcho@lanl.gov (J.H. Cho), picraux@lanl.gov (S.T. Picraux).

0378-7753/$ – see front matter © 2012 Elsevier B.V. All rights reserved.
doi:10.1016/j.jpowsour.2012.01.037

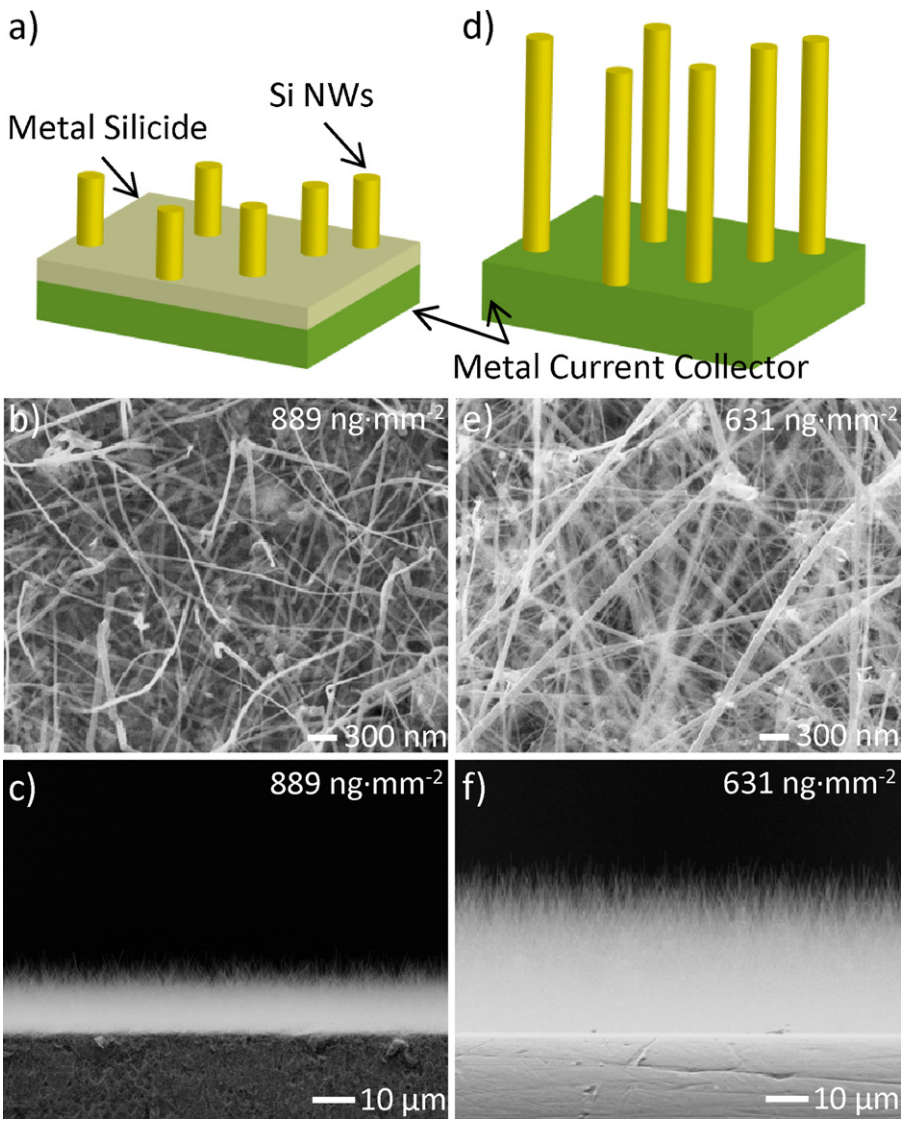

Fig. 1. (a, d) Schematic diagrams and (b, c, e, f) SEM images of SiNWs grown on a metal current collector (304 stainless steel) under different CVD growth conditions. (a–c) Metal silicides were formed during SiNW growth and showed higher mass gain and lower nanowire density than (d–f) that of silicon nanowires grown without metal silicide formation.

this electrode interaction effect is eliminated. Of particular significance a rate capability of 1912 and 997 mA h g^{-1} is observed at 10 C (42 A g^{-1}) and 20 C (84 A g^{-1}), respectively, for high-purity silicon nanowires, which is much higher than reported previously [4,8,9].

Silicide formation on the current collector decreases the weight percent (wt%) of SiNWs and leads to a lower density of SiNWs. Fig. 1a–c (case 1) and d–f (case 2) shows SiNWs grown on a stainless steel substrate under different CVD growth conditions, with a weight gain after growth of 889 ng mm^{-2} and 631 ng mm^{-2}, respectively. Although the weight gain of case 1 shown in Fig. 1a–c is higher than that of case 2 shown in Fig. 1d–f, the SiNW density of case 1 is less than that of case 2 due to metal silicide formation which increases the total weight. A problem with the metal silicide formation is that Si which would otherwise contribute to SiNW formation is consumed and the overall specific capacity of a silicon nanowire-based anode material is reduced. The specific capacity of the metal silicides is generally one to two orders of magnitude less than silicon capacity ($NiSi_2$: 327 mA h g^{-1}, $FeSi_2$: 65 mA h g^{-1}, $TiSi_2$: 27 mA h g^{-1} [10], and $CoSi_2$: 58 mA h g^{-1} [11]) thus lowering the overall anode capacity. In order to enhance the specific capacities of the metal silicides, various nanostructured anodes; such as nickel silicide (Ni_xSi_y) in the form of nanobelts (400 mA h g^{-1}), nanosheets (540 mA h g^{-1}) [12], and $FeSi_2$ (~580 mA h g^{-1}) in the form of nanocrystalline powder [13], have been explored. However, these values are still much lower than that of Si. Although silicon shows the highest gravimetric capacity, the resulting reduced weight percent of silicon nanowire due to metal silicide formation on the substrates (current collectors) leads to reduced overall capacities as given by

$$\text{overall specific capacity} = \frac{\text{total capacity}}{\text{total weight}} = \frac{C_{Si} \cdot W_{Si} + C_{MS} \cdot W_{MS}}{W_{Si} + W_{MS}} \quad (1)$$

where C_{Si} and C_{MS} are the silicon capacity and metal silicide capacity and W_{Si} and W_{MS} are the silicon weight and metal silicide weight, respectively. In order to enhance the overall specific capacity, the weight percent of active materials having high capacity (SiNWs) should be maximized and the weight percent of unwanted low specific capacity material (in this case metal silicides: W_{MS}) should be minimized. However, it is not easy to avoid the metal

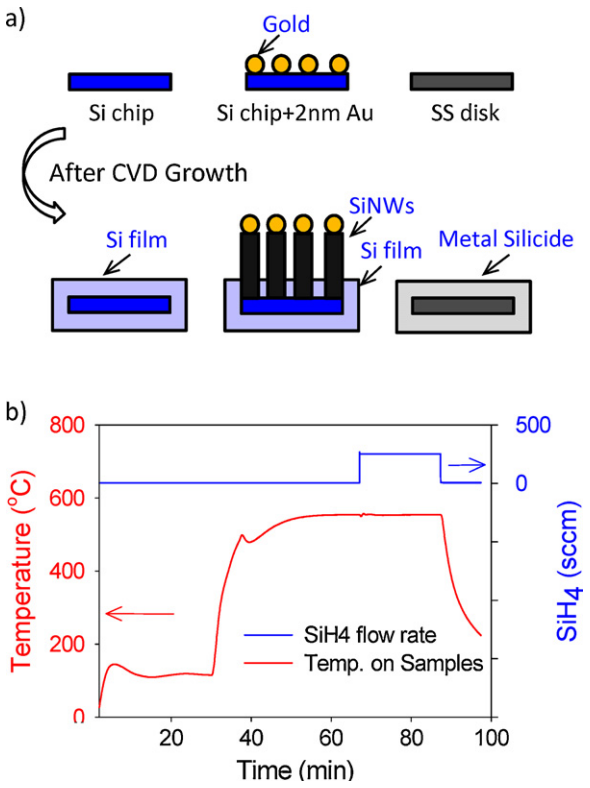

Fig. 2. A control experiment with three different substrates. (a) The different substrates were loaded into a CVD reactor together, and Si film, SiNWs, and metal silicide were formed on the substrates during CVD processing. (b) The temperature and SiH_4 gas flow vs. time profiles for the CVD process.

silicide formation during the CVD process at the SiNW growth temperature (500–900 °C) [14–17] because silicide formation temperatures range in or below the SiNW growth temperature range. For example, SiNW growth was attempted on commonly used copper current collectors, however, very poor nucleation of SiNW growth was observed due to strong wetting of the Au on the copper and at the same time extremely thick layer of copper silicide formed at the NW growth temperatures. In fact it is well known that silicon easily reacts with most transition metals (e.g., Ni, Pt, W, Cu, Cr, Ti, Co, Mo, Ta, Fe, Ir, Pd, etc.) over a wide temperature range to form silicides [18–23]. Fe_3Si, for example, is the first phase to form during low-temperature annealing (75–175 °C) and FeSi and $FeSi_2$ form at 350–450 °C and 550–650 °C, respectively [24]. However, it is possible to minimize the weight percent of metal silicide and maximize the weight percent of SiNWs through optimizing CVD growth temperature.

2. Experimental

In order to quantitatively characterize competing metal silicide and SiNW formation, a control experiment was first carried out with three different substrates: Si chips, Si chips with a 2 nm thick gold (Au) catalyst which was deposited using an electron beam (e-beam) evaporator, and polished 304 stainless steel (SS) disks (Fig. 2a). The three different substrates were loaded into a cold wall low pressure CVD reactor together and the samples were heated to a SiNW growth temperature. Once the temperature was stabilized, silane (50% SiH_4 in H_2) and doping gas (100 ppm phosphine) were introduced with the flow rates of 250 sccm and 100 sccm, respectively, and a chamber pressure of 3 Torr for 20 min (Fig. 2b). During the CVD process, only silicon (Si) film was deposited on the Si chip without metal silicide formation and SiNW growth because no catalyst was present for SiNW growth and no metal for metal silicide formation (Fig. 2a). On the other hand, SiNWs were grown with Si film deposition on a Si chip which has 2 nm thick Au catalyst for SiNW growth. On a stainless steel (SS) disk, metal silicide formed without SiNW growth because there was no Au catalyst. The weight gain of Si film, SiNWs, and metal silicide per unit area (mm^2) were obtained by measuring the weight change of the samples before and after a CVD process using a microbalance (Sartarious SE2: 0.1 μg resolution). We could directly measure the weight ($\mu g\,mm^{-2}$) of Si film from the Si chip sample. The weight of SiNWs was obtained from the weight change of a Si chip with Au catalyst after subtracting the weight of Si film which was measured from a Si chip sample without Au catalyst. The weight of metal silicide was determined from the weight change of the SS disk. Three identical samples for each substrate were prepared, and the average areal mass gains ($\mu g\,mm^{-2}$) of the each three materials (Si film, SiNWs, and metal silicide) were obtained after CVD processing for different growth temperatures.

To directly observe the metal silicide formation, we used Secondary Ion Mass Spectrometry (SIMS) with an Atomika 4500 quadrupole and obtained the metal silicide depth profiles. An oxygen primary ion beam was used for sputtering the stainless steel (SS) surface while positive secondary ions were recorded. The primary beam was at near normal incidence in order to minimize sample roughening artifacts. The beam was raster scanned over a $120 \times 120\,\mu m^2$. The depth scale was calculated by measuring the total crater depth using a Tencor surface profiler and assuming a uniform erosion rate.

In order to grow SiNWs with minimized metal silicide formation on 304 stainless steel (SS) disks, SS disks were polished with 400, 600, 800, 1200 grit paper, followed by solvent rinsing and 2 nm thick gold (Au) catalyst deposition using an electron beam (e-beam) evaporator. The SS disks were loaded into a cold wall low pressure CVD reactor at a base pressure of 1.0×10^{-6} Torr and the samples were heated to 120 °C for 30 min. After that, silane (50% SiH_4/H_2) and doping gas (100 ppm phosphine) were introduced with the flow rate of 250 sccm and 100 sccm, respectively, with a chamber pressure of 3 Torr. During the gas flow, the temperature was increased up to growth temperatures and maintained for 30 min. At the conclusion of growth all gases were closed and temperature was set to room temperature. Based on our nanowire device studies the resulting n-type doping concentration is estimated to be $>10^{19}\,cm^{-3}$.

Coin-type half cells (2032 size) were assembled in a helium-filled glove box under less than 0.5 ppm oxygen and 0.5 ppm moisture environments. The cells consisted of SiNW active materials which were directly grown on a 304 stainless steel disk, a 25 μm thick microporous monolayer membrane as a separator (Celgard, 2400), a 1.5 mm thick lithium foil as reference and counter electrodes (Alfa Aesar), and electrolyte (Novolyte). The electrolyte was 1 M lithium hexafluorophosphate ($LiPF_6$) in 1:2 mixture of ethylene carbonate (EC) and dimethyl carbonate (DMC). Electrochemical performances were carried out using a multichannel potentiostat (Bio-Logic, VMP3) with a constant current mode within the voltage range of 0.02–1.5 V vs. Li/Li^+ and current and voltage data were collected at every 5 mV changes. All the samples were cycled at a low rate, 0.05 C (1 C = 4200 mA g^{-1}) in the first cycle (both lithiation and delithiation) in order to stabilize anode materials and then the cycle rate was increased in the remaining cycles.

3. Results and discussion

Fig. 3a shows the areal mass gain of the materials at different growth temperatures. As the temperature was increased, the areal mass gains of the three materials increased with the Si film showing

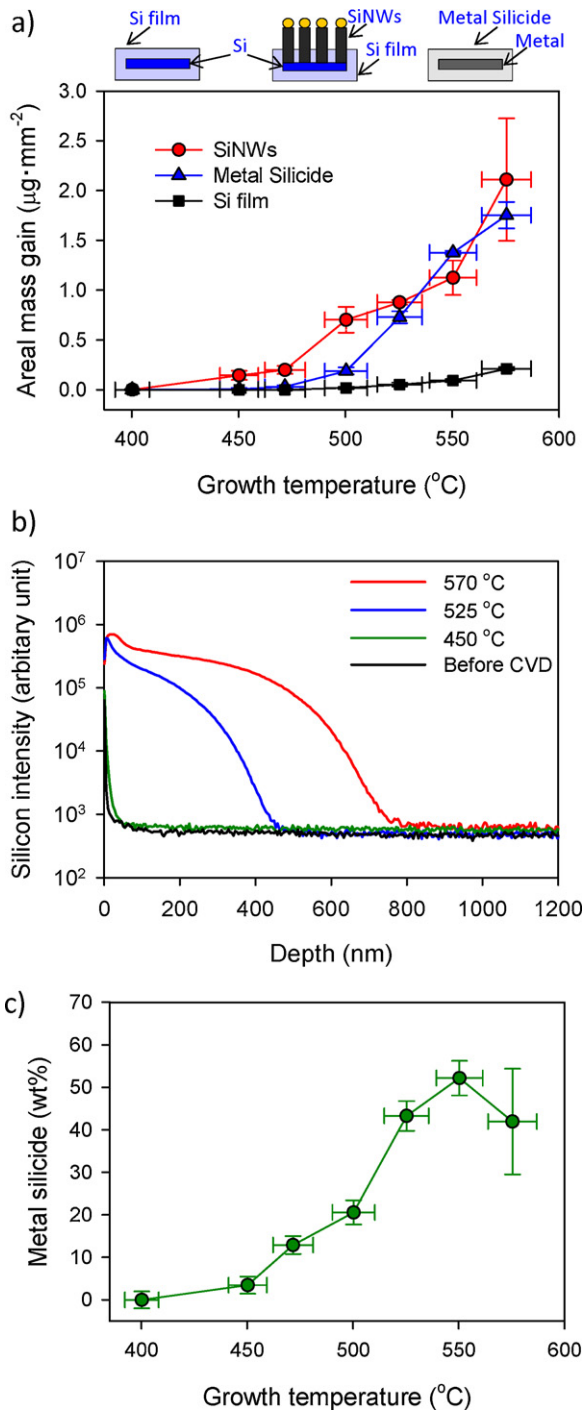

Fig. 3. (a) Areal mass gain of SiNWs, metal silicide, and Si film vs. growth temperatures. (b) Secondary Ion Mass Spectrometry (SIMS) depth profile of Si from SS surfaces before and after CVD process at 450, 525, and 570 °C. One sample was characterized without CVD processing, and three samples were separately loaded into a CVD system. And then the each samples were heated to three different CVD growth temperatures, 450, 525, and 570 °C, respectively, with the flow of silane and doping gas. (c) Weight percent of metal silicide vs. growth temperatures which were obtained based on the data shown in Fig. 3a.

the lowest growth rate. The overall mass gain of SiNWs was higher than that of metal silicide, and no mass gain could be observed from all materials below 400 °C for a microbalance with 0.1 μg resolution capability. Metal silicide and SiNWs showed mass gain from 450 °C, but Si film did not show mass gain until 500 °C. Weight gains above 600 °C were not measured because delamination of the metal silicide film occurred from the 304 stainless steel (SS) disks during the CVD process due to excessive Si-rich metal silicide formation. The Si-rich metal silicide layer induces high compressive film stress [25,26], and the high stress caused the metal silicide to buckle and delaminate. The depth profiles of Si from the SS surfaces were obtained before and after CVD processing at 450, 525, and 570 °C for 20 min with a Secondary Ion Mass Spectrometry (SIMS) in order to verify the metal silicide formation and characterize the silicide thickness formed at three different CVD growth temperatures (Fig. 3b). As shown in the figure, the depth of metal silicide is deeper with increasing CVD growth temperature. This result is consistent with our indirect observation of increasing mass gain with growth temperature (Fig. 3a). CVD processing at 570 and 525 °C shows the Si signals extend to a depth of 800 nm and 500 nm, respectively, indicating the parasitic silicide reactions are significant at typical SiNW growth temperatures. A sample processed at 450 °C shows very shallow metal silicide formation (40 nm deep) and low signal intensity compared to the other two samples processed at 525 and 570 °C. Moreover, the depth profiles for 450 °C are very similar to that of the samples before CVD processing. This means an extremely small amount of metal silicide forms at or below this temperature (450 °C).

Based on the measured areal mass gains of metal silicide (AMG_{MS}), SiNWs (AMG_{SiNWs}), and Si film (AMG_{SiFm}) shown in Fig. 3a, the weight percents (wt%) of metal silicide vs. growth temperatures were obtained by

$$\text{wt\% of metal silicide} = \frac{AMG_{MS}}{AMG_{MS} + AMG_{SiNWs} + AMG_{SiFm}} \times 100 \quad (2)$$

Fig. 3c shows the result which shows a parabolic increase in silicide formation with growth temperature followed by a maximum at 550 °C. In order to reduce metal silicide formation on the SS current collectors, one needs to avoid SiNW growth at 550 °C and grow at low temperatures. However growth should be higher than 400 °C because there is no metal silicide formation ($AMG_{MS} \approx 0$) as well as no SiNW growth ($AMG_{SiNW} \approx 0$) at or below 400 °C.

The content of metal silicide on metal current collectors could be controlled with the results of Fig. 3c, and three samples with different proportions of metal silicide (~0.6 wt% metal silicide with ~99.4 wt% SiNWs (wt_{Si}), ~40 wt% metal silicide with ~60 wt% SiNWs ($wt_{MS/Si}$), and ~100 wt% metal silicide (wt_{MS})), were prepared to study the effect of metal silicide formation on a SiNW-based Li-ion battery anode capacity. All samples were prepared on SS disks, and the ~100 wt% metal silicide without SiNW growth sample was prepared at a 510 °C growth temperature using no Au catalyst. Coin-type half cells (2032 size) were assembled and the electrochemical performances of the three samples, 0.6 wt% metal silicide/99.4 wt% SiNWs (wt_{Si}), 40 wt% metal silicide/60 wt% SiNWs ($wt_{MS/Si}$), and 100 wt% metal silicide (wt_{MS}), studied (Fig. 4). The differential capacity curves for the three samples (wt_{Si}, $wt_{MS/Si}$, and wt_{MS}) captured after 2nd cycle at 0.5 C (0.5 C = 2100 mA g^{-1}) showed two major lithiation peaks near 200 mV and 40 mV and two major delithiation peaks near 500 mV and 300 mV, which are in agreement with previous reports [27,28]. We did not observed a large lithiation and delithiation potential difference in the three samples from the differential capacity curves. However, we observed that the differential capacity of wt_{Si} is one order of magnitude higher than that of wt_{MS} as shown in Fig. 4a due to the large portion of anode material (99.4 wt% Si) which is more highly reactive with Li than metal silicide. The magnitude of differential capacity of $wt_{MS/Si}$ is intermediate between that of wt_{Si} and wt_{MS} because of coexistence of silicon nanowires (60 wt%) and metal silicide (40 wt%). Galvanostatic charge–discharge profiles (Fig. 4b) as well as specific capacity and Coulombic efficiency vs. cycle number (Fig. 4c) generated by wt_{Si}, $wt_{MS/Si}$, and wt_{MS} were collected between 20 mV and 1.5 V at a constant current

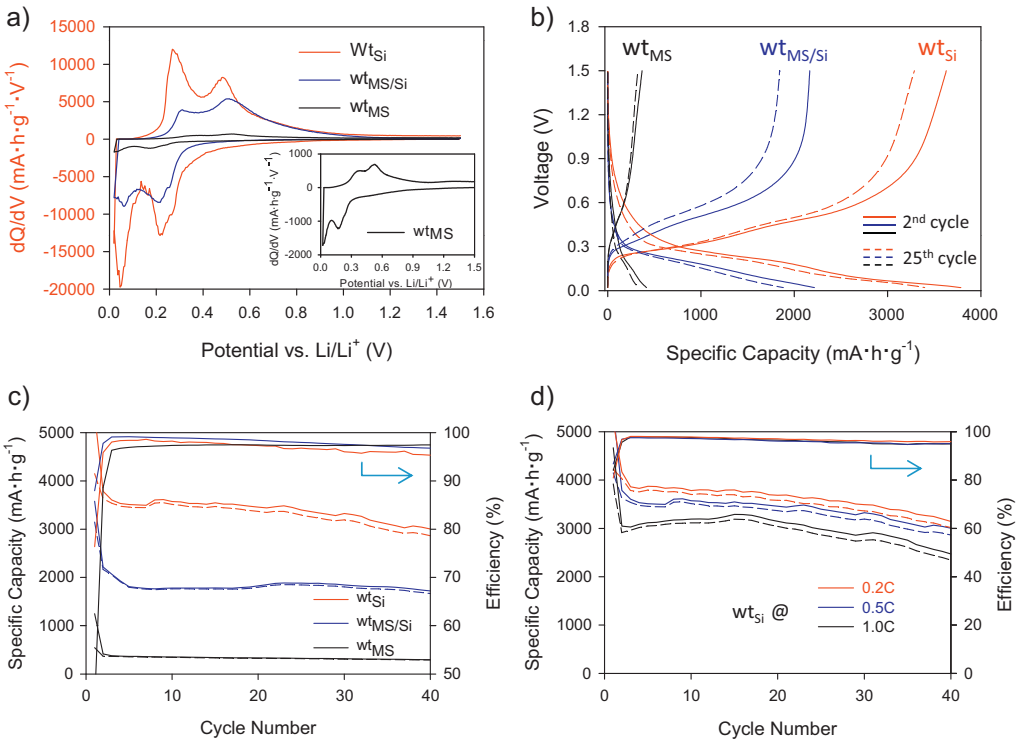

Fig. 4. Electrochemical performances of three samples, 0.6 wt% metal silicide/99.4 wt% SiNWs (wt_{Si}), 40 wt% metal silicide/60 wt% SiNWs ($wt_{MS/Si}$), and 100 wt% metal silicide (wt_{MS}). (a) Differential capacity curves captured after 2nd cycle at 0.5 C. Inset: a magnified differential capacity curve of wt_{MS}. (b) Galvanostatic charge–discharge profiles for 2nd and 25th cycles. (c) Specific capacity and Coulombic efficiency vs. cycle number collected between 20 mV and 1.5 V at a constant current rate of 0.05 C in the first cycle and 0.5 C in the remaining cycles. (d) The specific charge/discharge capacities and Coulombic efficiency of wt_{Si} vs. cycle number at the cycle rates of 0.2, 0.5, and 1.0 C.

rate of 0.05 C in the first cycle and 0.5 C in the remaining cycles. The specific charge (lithiation) and discharge (delithiation) capacities of wt_{Si} were 3786 and 3629 mA h g^{-1} at 2nd cycle with 0.5 C rate, respectively, and the specific capacities were maintained over 3400 mA h g^{-1} until 25 cycles (Fig. 4b).

The specific charge and discharge capacities observed at a 0.2 C rate for Si (wt_{Si}) of 3871 and 3793 mA h g^{-1} (Fig. 4d) after 5 cycles are the highest values ever reported for silicon nanowire anodes grown directly on metal current collectors. We note that here we have used the total weights of the active materials including metal silicide for specific capacity determinations (i.e. without subtracting the metal silicide weight gain from the total weight gain after CVD growth). The average specific capacities of wt_{Si} over 40 cycles are 3670 (charge) and 3537 mA h g^{-1} (discharge) at 0.2 C (Fig. 4d) and 3448 (charge) and 3319 mA h g^{-1} (discharge) at 0.5 C which are one order magnitude higher than that of wt_{MS} (charge: 357 mA h g^{-1}, discharge: 329 mA h g^{-1} at 0.5 C) and twice as high as that of the 40% metal silicide, $wt_{MS/Si}$, sample (charge: 1874 mA h g^{-1}, discharge: 1830 mA h g^{-1}) (Fig. 4c). Although the present specific capacity of wt_{MS} in thin film form is significantly higher than previous reports [10,11], it is still one order of magnitude smaller than that of wt_{Si}. These results show that metal silicide formation with its low specific capacity for Li storage reduces overall specific capacity of a silicon nanowire-based lithium-ion battery anode. We note that relatively low Coulombic efficiencies (95.9–98.1%) and cycling capacity retention (Fig. 4d) are obtained in these measurements and understanding the influence of various parameters on low Coulombic efficiencies and capacity retention is an ongoing area of research.

In order to enhance specific capacity, the weight percent of an anode material having high specific capacity should be maximized while that of any poorly reactive anode material with Li should be minimized provided the poorly reactive anode material does not have any additional hybrid function to enhance battery performance, such as cyclability or power density. To systematically explore such optimization for the influence of metal silicide formation on overall specific capacity we carried out the experiments and analysis shown in Fig. 5. Two samples (wt_{Si} and wt_{MS}) were prepared and cycled at 0.05, 0.1, and 0.25 C in the first, second, and third cycle, respectively, and the remaining cycles were cycled with increasement of 0.25 C up to 20.0 C. Fig. 5a shows charging and discharging cycles of wt_{Si} which was cycled until a rate of 20.0 C. Fig. 5b shows discharge capacities (delithiation) vs. cycle rate (0.1–20.0 C) of wt_{Si} and wt_{MS}, with the inset showing the galvanostatic charge/discharge profiles of wt_{Si} between 0.02 and 1.5 V vs. Li/Li^+ at a rate of 0.1, 1.0, 10.0, and 20.0 C. The discharge capacities of wt_{Si} (the sample minimized metal silicide: 0.6 wt%) at 10.0 C (42 A g^{-1}) and 20.0 C (84 A g^{-1}) were 1912 and 997 mA h g^{-1} (Fig. 5b). We note that SiNWs with minimized metal silicide (high-purity silicon nanowires) reach extremely high capacities at high cycle rates and these values are much higher than those reported previously [4,8,9]. On the other hand, the discharge capacities of wt_{MS} (100 wt% metal silicide) showed very low capacities at the high cycle rates (44 and 15 mA h g^{-1} at 10.0 and 20.0 C, respectively). Based on Eq. (1) and the experimental data (specific discharge capacity measurements of wt_{Si} and wt_{MS} at different cycle rates) of Fig. 5b, the results given in Fig. 5c and d were obtained. These plots show the influence of metal silicide formation on overall specific capacity. An anode material with 50 wt% metal silicide, for example, reduces about half of the overall capacity of silicon nanowire-based anodes (~100 wt% SiNWs) (Fig. 5c). Although Fig. 5c uses only two experimental conditions of silicide formation (specific capacities for 0.6 and 100 wt% metal silicide) at each cycle rate and the specific capacities were linearized, we verified the predicted data is in good agreement with the experiment data for the measured specific capacity at 40 wt% metal silicide and 0.5 C

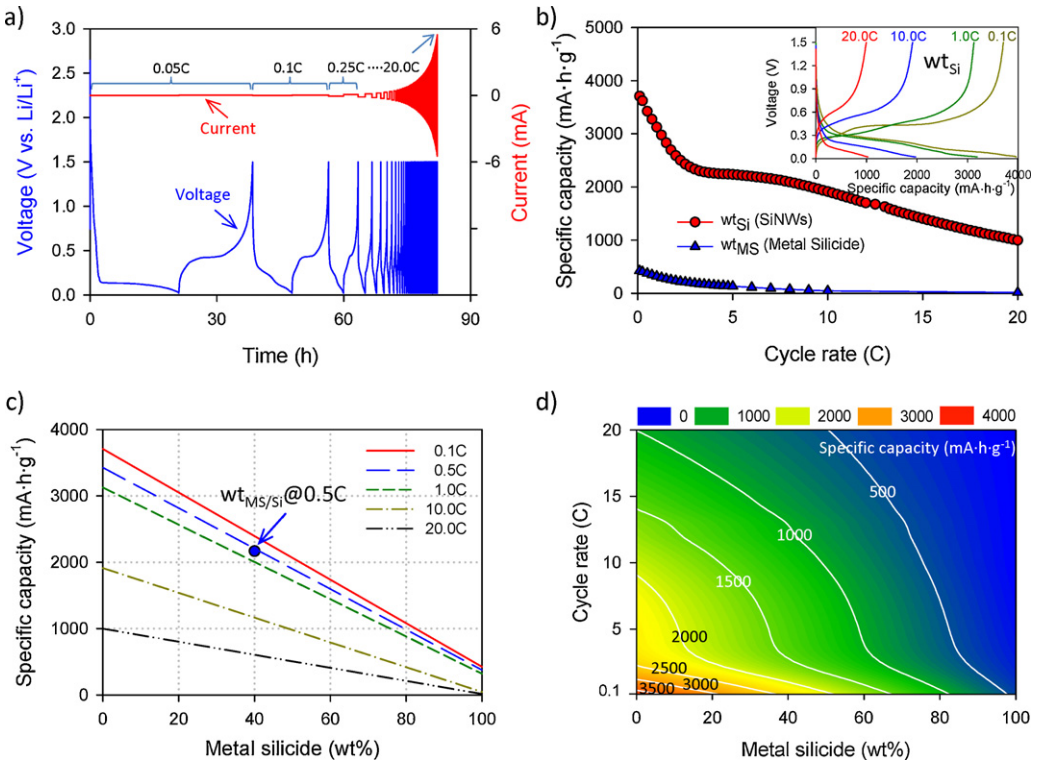

Fig. 5. The effect of metal silicide formation on silicon nanowire-based lithium-ion battery anode capacity. (a) Voltage and current signals of wt_{Si} during charge and discharge. The sample was cycled at increasing rates of 0.05, 0.1, and 0.25 C for the first 3 cycles and then the rate was increased by 0.25 C for successive cycles until the rate of 20.0 C was reached. (b) Discharge capacities vs. cycle rate (0.1–20.0 C) of wt_{Si} and wt_{MS}. Inset: galvanostatic charge/discharge profile of wt_{Si} between 0.02 and 1.5 V vs. Li/Li^+ at a rate of 0.1, 1.0, 10.0, and 20.0 C. (c) Overall specific capacity of a silicon nanowire-based anode vs. weight percent of metal silicide at 0.1, 0.5, 1.0, 10.0, and 20.0 C rates. (d) Contour plot showing specific capacities as a function of weight percent of metal silicide for the indicated cycle rates.

taken in the second cycle (filled circle in Fig. 5c). As is illustrated in the contour plots of Fig. 5d, minimizing the metal silicide formation not only enhances overall specific capacity but also improves the rate capability. For example, the discharge capacity of a sample (33 wt% SiNWs and 67 wt% metal silicide) reached 1500 mA h g^{-1} at low cycle rate of 0.1 C. However, once we minimize the metal silicide formation close to zero, the specific capacity of 1500 mA h g^{-1} was achieved at 14.0 C (Fig. 5d).

4. Conclusion

Here we have demonstrated that the effect of metal silicide formation on the rate capability and overall specific capacity of silicon nanowire-based Li ion anodes grown on stainless steel substrates using a CVD processing. The metal silicide forms during the CVD process for SiNW growth at high temperature and reduces overall specific capacity. The performance of a silicon nanowire-based lithium-ion battery anode is shown to be greatly improved by optimizing the SiNW growth temperature to minimize metal silicide formation. Minimizing silicide formation shows that silicon nanowires not only have enhanced the overall specific capacity from that previously reported, but also that charge–discharge rate capacities are significantly increased. These results demonstrate the important role of nanomaterials synthesis (e.g., purity issue) for the design of high performance batteries implemented by nanostructured silicon and/or silicon-based composite anodes.

Acknowledgments

This material is based upon work supported as part of the Nanostructures for Electrical Energy Storage, an Energy Frontier Research Center funded by the U.S. Department of Energy, Office of Science, Office of Basic Energy Sciences under Award Number DESC0001160. The work was performed, in part, at the Center for Integrated Nanotechnologies, a U.S. Department of Energy, Office of Basic Energy Sciences user facility. Los Alamos National Laboratory, an affirmative action equal opportunity employer, is operated by Los Alamos National Security, LLC, for the National Nuclear Security Administration of the U.S. Department of Energy under contract DE-AC52-06NA25396.

References

[1] V. Manev, I. Naidenov, B. Puresheva, P. Zlatilova, G. Pistoia, J. Power Sources 55 (1995) 211.
[2] B.A. Boukamp, G.C. Lesh, R.A. Huggins, J. Electrochem. Soc. 128 (1981) 725.
[3] L.Y. Beaulieu, K.W. Eberman, R.L. Turner, L.J. Krause, J.R. Dahn, Electrochem, Solid State Lett. 4 (2001) A137.
[4] C.K. Chan, H. Peng, G. Liu, K. McIlwrath, X.F. Zhang, R.A. Huggins, Y. Cui, Nat. Nanotechnol. 3 (2008) 31.
[5] K. Kang, H.S. Lee, D.W. Han, G.S. Kim, D. Lee, G. Lee, Y.M. Kang, M.H. Jo, Appl. Phys. Lett. 96 (2010) 053110.
[6] L.F. Cui, R. Ruffo, C.K. Chan, H. Peng, Y. Cui, Nano Lett. 9 (2009) 491.
[7] H. Kim, J. Cho, Nano Lett. 8 (2008) 3688.
[8] X. Chen, K. Gerasopoulos, J. Guo, A. Brown, R. Ghodssi, J.N. Culver, C. Wang, Electrochim. Acta 56 (2011) 5210.
[9] Y. Yao, M.T. McDowell, I. Ryu, H. Wu, N. Liu, L. Hu, W.D. Nix, Y. Cui, Nano Lett. 11 (2011) 2949.
[10] A. Netz, R.A. Huggins, W. Weppner, Ionics 7 (2001) 433.
[11] A. Netz, R.A. Huggins, Solid State Ionics 175 (2004) 215.
[12] H.L. Zhang, F. Li, C. Liu, H.M. Cheng, Nanotechnology 19 (2008) 165606.
[13] J.H. Ahn, G.X. Wang, H.K. Liu, S.X. Dou, Mater Sci. Forum 360–362 (2001) 595.
[14] K. Jun, J.M. Jacobson, Nano Lett. 10 (2010) 2777.
[15] A.I. Hochbaum, R. Fan, R. He, P. Yang, Nano Lett. 5 (2005) 457.
[16] X.H. Liu, L.Q. Zhang, L. Zhong, Y. Liu, H. Zheng, J.W. Wang, J.H. Cho, S.A. Dayeh, S.T. Picraux, J.P. Sullivan, S.X. Mao, Z.Z. Ye, J.Y. Huang, Nano Lett. 11 (2011) 2251.
[17] C.K. Chan, R. Ruffo, S.S. Hong, R.A. Huggins, Y. Cui, J. Power Sources 189 (2009) 34.
[18] Q.G. Zhu, H. Iwasaki, E. Williams, R.L. Park, J. Appl. Phys. 60 (1986) 2629.
[19] C.S. Lee, H. Gong, R. Liu, A.T.S. Wee, C.L. Cha, A. See, L. Chan, J. Appl. Phys. 90 (2001) 3822.

[20] S.P. Murarka, D.B. Fraser, J. Appl. Phys. 51 (1980) 1593.
[21] T. Rodrígueza, A. Almendraa, M.F. da Silvab, J.C. Soaresc, H. Woltersc, A. Rodrígueza, J. Sanz-Maudesa, Nucl. Instrum. Methods B 113 (1996) 279.
[22] Y.U. Idzerda, E.D. Williams, R.L. Park, J. Vähäkangas, Surf. Sci. 177 (1986) L1028.
[23] M. Ohring, Materials Science of Thin Films, 2nd, 2002, p. 693.
[24] J.M. Gallego, J.M. García, J. Alvarez, R. Miranda, Phys. Rev. B 46 (1992) 13339.
[25] A.H. Reader, A.H. Ommen, P.J.W. Weijs, R.A.M. Wolter, D.J. Oostra, Rep. Prog. Phys. 56 (1992) 1397.
[26] J.T. Pan, L. Blech, J. Appl. Phys. 55 (1984) 2874.
[27] S. Ohara, J. Suzuki, K. Sekine, T. Takamura, J. Power Sources 119–121 (2003) 591.
[28] W. Wang, P.N. Kumta, ACS Nano 4 (2010) 2233.